# Measurement of Proton, Nitrogen, and Carbonyl Chemical Shielding Anisotropies in a Protein Dissolved in a Dilute Liquid Crystalline Phase

**Gabriel Cornilescu[†,‡] and Ad Bax*[,†]**

*Contribution from the Laboratory of Chemical Physics, Building 5, National Institute of Diabetes and Digestive and Kidney Diseases, and Joined Biophysics Graduate Program of the University of Maryland and the National Institutes of Health, National Institutes of Health, Bethesda, Maryland 20892-0520*

*Received May 11, 2000. Revised Manuscript Received August 1, 2000*

**Abstract:** The changes in a solute's chemical shifts between an isotropic and a liquid crystalline phase provide information on the magnitude and orientation of the chemical shielding tensors relative to the molecule's alignment frame. Such chemical shift changes have been measured for the polypeptide backbone C′, N, and $H^N$ resonances in the protein ubiquitin. Perdeuterated ubiquitin was dissolved in a medium containing a small volume fraction of phospholipid bicelles, which switches from an isotropic to a liquid crystalline phase at ca. 25 °C. The one-bond $^1H-^{15}N$ dipolar couplings provide a reference to determine the protein alignment tensor, using a vibrationally corrected $^1H-^{15}N$ bond length of 1.04 Å, corresponding to $r_{CN} = 1.33$ Å. Assuming all atoms of a given type have the same chemical shielding anisotropy (CSA) tensor, the average C′ tensor values are $\sigma_{11} = -75$ ppm, $\sigma_{22} = -12$ ppm, and $\sigma_{33} = 87$ ppm for $^{13}C'$ with an angle between $\sigma_{11}$ and the C′−N bond of 38°, and $\sigma_{33}$ orthogonal to the peptide plane. Similarly, for $^{15}N$, $\sigma_{11} = -108$ ppm, $\sigma_{22} = 46$ ppm, and $\sigma_{33} = 63$ ppm, with an angle of 19° between the H−N vector and the $\sigma_{11}$ axis, and $\sigma_{22}$ orthogonal to the peptide plane. For $H^N$, the commonly used approximation of an axially symmetric shielding tensor is found to be invalid, and best fit tensor values are $\sigma_{11} = -6$ ppm, $\sigma_{22} = 0$ ppm, and $\sigma_{33} = 6$ ppm, with the $\sigma_{11}$ axis orthogonal to the peptide plane and $\sigma_{33}$ roughly parallel to the H−N bond vector. Considerable differences in CSA are found when separately considering residues in helical and extended regions of the polypeptide chain. For $^{13}C'$ and $^{15}N$, the scatter in the correlation between experimental chemical shift changes and those predicted on the basis of the structure and a uniform CSA tensor is dominated by uncertainty in the protein structure and by the fact that the uniform CSA assumption is not valid. Upper limits for the degree of this intrinsic variation in the CSA tensor are obtained from these correlations. For $^1H^N$, the scatter is completely dominated by intrinsic variations in the CSA tensor at the different sites.

## Introduction

Chemical shielding anisotropy (CSA) is a key parameter in structure determination by solid-state NMR.[1−8] CSA also plays a key role in $^{15}N$ and $^{13}C'$ relaxation studies, where accurate knowledge of the corresponding tensors is a prerequisite for quantitative interpretation of relaxation rates in terms of backbone dynamics, especially when considering anisotropic internal motion.[9−12] Relaxation interference between CSA and dipolar terms contains important angular information,[13−17] and also forms the basis of so-called TROSY experiments where the effect is exploited to increase resolution in spectra of slowly tumbling biological macromolecules.[18−20]

* Address correspondence to this author. Laboratory of Chemical Physics, Building 5, Room 126, NIH, Bethesda, MD 20892-0520. E-mail: bax@nih.gov. Phone: 301 496 2848. FAX: 301 402 0907.

† Laboratory of Chemical Physics.

‡ Joined Biophysics Graduate Program of the University of Maryland and the National Institutes of Health.

(1) Mai, W.; Hu, W.; Wang, C.; Cross, T. A. *Protein Sci.* **1993**, *2*, 532−542.

(2) Ketchem, R. R.; Lee, K. C.; Huo, S.; Cross, T. A. *J. Biomol. NMR* **1996**, *8*, 1−14.

(3) Feng, X.; Eden, M.; Brinkmann, A.; Luthman, H.; Eriksson, L.; Graslund, A.; Antzutkin, O. N.; Levitt, M. H. *J. Am. Chem. Soc.* **1997**, *119*, 12006−12007.

(4) Marassi, F. M.; Opella, S. J. *Curr. Opin. Struct. Biol.* **1998**, *8*, 640−648.

(5) Long, H. W.; Tycko, R. *J. Am. Chem. Soc.* **1998**, *120*, 7039−7048.

(6) Marassi, F. M.; Ma, C.; Gesell, J. J.; Opella, S. J. *Appl. Magn. Reson.* **1999**, *17*, 433−447.

(7) Fu, R. Q.; Cross, T. A. *Annu. Rev. Biophys. Biomol. Struct.* **1999**, *28*, 235−268.

(8) Ishii, Y.; Tycko, R. *J. Am. Chem. Soc.* **2000**, *122*, 1443−1455.

(9) Lienin, S. F.; Bremi, T.; Brutscher, B.; Bruschweiler, R.; Ernst, R. R. *J. Am. Chem. Soc.* **1998**, *120*, 9870−9879.

(10) Scheurer, C.; Skrynnikov, N. R.; Lienin, S. F.; Straus, S. K.; Bruschweiler, R.; Ernst, R. R. *J. Am. Chem. Soc.* **1999**, *121*, 4242−4251.

(11) Fischer, M. W. F.; Zeng, L.; Majumdar, A.; Zuiderweg, E. R. P. *Proc. Natl. Acad. Sci. U.S.A.* **1998**, *95*, 8016−8019.

(12) Fischer, M. W. F.; Majumdar, A.; Zuiderweg, E. R. P. *Prog. Nucl. Magn. Reson. Spectrosc.* **1998**, *33*, 207−272.

(13) Reif, B.; Hennig, M.; Griesinger, C. *Science* **1997**, *276*, 1230−1233.

(14) Yang, D. W.; Kay, L. E. *J. Am. Chem. Soc.* **1998**, *120*, 9880−9887.

(15) Reif, B.; Steinhagen, H.; Junker, B.; Reggelin, M.; Griesinger, C. *Angew. Chem., Int. Ed.* **1998**, *37*, 1903−1906.

(16) Brutscher, B.; Skrynnikov, N. R.; Bremi, T.; Bruschweiler, R.; Ernst, R. R. *J. Magn. Reson.* **1998**, *130*, 346−351.

(17) Chiarparin, E.; Pelupessy, P.; Ghose, R.; Bodenhausen, G. *J. Am. Chem. Soc.* **2000**, *122*, 1758−1761.

(18) Pervushin, K.; Riek, R.; Wider, G.; Wuthrich, K. *Proc. Natl. Acad. Sci. U.S.A.* **1997**, *94*, 12366−12371.

(19) Yang, D. W.; Kay, L. E. *J. Am. Chem. Soc.* **1999**, *121*, 2571−2575.

(20) Salzmann, M.; Wider, G.; Pervushin, K.; Senn, H.; Wuthrich, K. *J. Am. Chem. Soc.* **1999**, *121*, 844−848.

10.1021/ja0016194 
Published on Web 09/30/2000

Improvements in both spectrometer hardware and measurement methods now permit relaxation rates to be measured at levels of accuracy where their quantitative interpretation is limited by the unknown degree of variation in the CSA from site to site. The CSA of the $^{15}N$, $^{1}H^{N}$, and $^{13}C'$ peptide backbone nuclei is known to depend on numerous parameters, including backbone geometry and hydrogen bonding.[21] Experimental approaches to measure individual CSA tensors from $^{15}N$ relaxation rates suggest considerable variation of this tensor.[22,23]

To date, information on the $^{15}N$ and $^{13}C'$ CSA tensor orientation and magnitude in peptide bonds has been obtained primarily from solid-state NMR measurements, either on amorphous powders, polycrystalline material, or polypeptides anchored in oriented bilayers.[24−33] For the backbone amide protons, $H^{N}$, accurate CSA measurements in proteins by solid-state NMR are very challenging, and so far have yielded only limited information. Nevertheless, knowledge of its tensor and understanding of its relation to structure is key to the use of the potentially very powerful PISEMA solid-state NMR experiment, which has been developed for the study of oriented membrane proteins.[34,35]

For all three types of nuclei, $^{15}N$, $^{13}C'$, and $^{1}H^{N}$, information on the CSA tensor has also become available from solution NMR relaxation studies of proteins. For $^{15}N$, analysis of the magnetic field dependence of the relaxation rates yielded a considerably (5−20%) higher CSA value (170−175 ppm) than observed in the solid state.[9,36,37] Independent support for these higher values is provided by recent relaxation interference experiments,[23,38] and by measurement of the change in $^{15}N$ chemical shift when a weak degree of alignment is imposed.[39,40] The discrepancy between solid-state and solution data has been attributed to the fact that the solution data have been corrected for the effects of internal motion, whereas solid-state values have been derived from the motionally narrowed powder patterns.[9,41] The effect of such motions is remarkably large, as evidenced by a 10−15% reduction in the one-bond $^{15}N-^{1}H$ dipolar coupling relative to the value expected for a static 1.02 Å N−H bond length.[34,42,43] For $^{15}N$ NMR studies of protein backbone motions, the CSA tensor is often assumed to be axially symmetric, although considerable asymmetries have been reported in CSA tensors measured by solid-state NMR.[27,33,43] Recently, large variations in this number from one site to another were calculated from measurements of cross correlations between $^{15}N$ CSA and the $^{1}H^{N}-^{15}N$ dipolar interaction and the rate of the $^{15}N$ transverse relaxation,[22] although this degree of variation is sensitive to the way in which the measurements and analyses are performed.[23] When quantitatively interpreting the effect of relaxation interference between $^{15}N$ CSA and one-bond $^{1}H^{N}-^{15}N$, not only the magnitude but also the orientation of the CSA tensor is important. Most literature estimates for the angle between the N−H bond and the unique axis of the CSA tensor fall in the 11° to 26° range.[25−33]

For backbone carbonyls, solution-state relaxation measurements also point to higher CSA values than observed in the solid state, but few data are available.[9,44] Accurate knowledge of the $^{13}C'$ CSA tensor and its degree of variation from one site to another is needed for quantitative interpretation of relaxation interference experiments, which can yield backbone torsion angle information in proteins.[14,16,17] Increased knowledge of $^{13}C'$ CSA orientation and magnitude not only offers the potential for improving the quality of structures determined by NMR, it also is essential for a more detailed analysis of dynamic processes by NMR relaxation. For example, when interpreting these relaxation times in terms of asymmetric motion, both the orientation and magnitude of the CSA tensor are critical.[9,45]

For amide protons, relaxation rates are usually dominated by homonuclear dipolar interactions and they are therefore only rarely interpreted in terms of a detailed dynamics model. However, relaxation interference between the $^{1}H^{N}$ CSA and the $^{1}H^{N}-^{15}N$ dipolar interaction can be used to negate the dipolar interaction and to obtain considerable line narrowing, particularly in proteins where all nonexchangeable protons are substituted by deuterons.[18] Knowledge of the $^{1}H^{N}$ CSA is important to predict at what field strength this line narrowing effect is optimized. For $^{1}H^{N}$, solution-state experiments that measure relaxation interference between the $^{1}H^{N}$ CSA and the $^{15}N-^{1}H$ dipolar coupling indicate a larger average CSA value for $\beta$-sheet residues than for $\alpha$-helical ones, but also show a significant degree of variation from one site to another.[46,47] This variation is responsible for the large range in $^{1}H^{N}$ line widths observed in TROSY spectra of perdeuterated proteins.[48] However, no information has been available on whether this variation is related to a change in orientation or magnitude of the CSA tensor. Finally, in solid-state NMR experiments on oriented samples, knowledge of the $^{1}H^{N}$ CSA tensor is important when interpreting the observed $^{1}H^{N}$ chemical shift in terms of orientation of the corresponding N−H bond.[34,35,49]

(21) Sitkoff, D.; Case, D. A. *Prog. Nucl. Magn. Reson. Spectrosc.* **1998**, *32*, 165−190.
(22) Fushman, D.; Tjandra, N.; Cowburn, D. *J. Am. Chem. Soc.* **1998**, *120*, 10947−10952.
(23) Kroenke, C. D.; Rance, M.; Palmer, A. G. *J. Am. Chem. Soc.* **1999**, *121*, 10119−10125.
(24) Duncan, T. M. *A Compilation of Chemical Shift Anisotropies*; Farragut Press: Madison, 1990.
(25) Teng, Q.; Iqbal, M.; Cross, T. A. *J. Am. Chem. Soc.* **1992**, *114*, 5312−5321.
(26) Oas, T. G.; Hartzell, C. J.; McMahon, T. J.; Drobny, G. P.; Dahlquist, F. W. *J. Am. Chem. Soc.* **1987**, *109*, 5956−5962.
(27) Oas, T. G.; Hartzell, C. J.; Dahlquist, F. W.; Drobny, G. P. *J. Am. Chem. Soc.* **1987**, *109*, 5962−5966.
(28) Lumsden, M. D.; Wasylishen, R. E.; Eichele, K.; Schindler, M.; Penner, G. H.; Power, W. P.; Curtis, R. D. *J. Am. Chem. Soc.* **1994**, *116*, 1403−1413.
(29) Hartzell, C. J.; Pratum, T. K.; Drobny, G. *J. Chem. Phys.* **1987**, *87*, 4324−4331.
(30) Hartzell, C. J.; Whitfield, M.; Oas, T. G.; Drobny, G. P. *J. Am. Chem. Soc.* **1987**, *109*, 5966−5969.
(31) Asakawa, N.; Takenoiri, M.; Sato, D.; Sakurai, M.; Inoue, Y. *Magn. Reson. Chem.* **1999**, *37*, 303−311.
(32) Shoji, A.; Ozaki, T.; Fujito, T.; Deguchi, K.; Ando, S.; Ando, I. *Macromolecules* **1989**, *22*, 2860−2863.
(33) Hiyama, Y.; Niu, C. H.; Silverton, J. V.; Bavoso, A.; Torchia, D. A. *J. Am. Chem. Soc.* **1988**, *110*, 2378−2383.
(34) Wu, C. H.; Ramamoorthy, A.; Gierasch, L. M.; Opella, S. J. *J. Am. Chem. Soc.* **1995**, *117*, 6148−6149.
(35) Gu, Z. T. T.; Opella, S. J. *J. Magn. Reson.* **1999**, *140*, 340−346.
(36) Tjandra, N.; Wingfield, P.; Stahl, S.; Bax, A. *J. Biomol. NMR* **1996**, *8*, 273−284.
(37) Fushman, D.; Tjandra, N.; Cowburn, D. *J. Am. Chem. Soc.* **1999**, *121*, 8577−8582.
(38) Tjandra, N.; Szabo, A.; Bax, A. *J. Am. Chem. Soc.* **1996**, *118*, 6986−6991.
(39) Ottiger, M.; Tjandra, N.; Bax, A. *J. Am. Chem. Soc.* **1997**, *119*, 9825−9830.
(40) Boyd, J.; Redfield, C. *J. Am. Chem. Soc.* **1999**, *121*, 7441−7442.
(41) Case, D. A. *J. Biomol. NMR* **1999**, *15*, 95−102.
(42) Roberts, J. E.; Harbison, G. S.; Munowitz, M. G.; Herzfeld, J.; Griffin, R. G. *J. Am. Chem. Soc.* **1987**, *109*, 4163−4169.
(43) Lee, D. K.; Wittebort, R. J.; Ramamoorthy, A. *J. Am. Chem. Soc.* **1998**, *120*, 8868−8874.
(44) Dayie, K. T.; Wagner, G. *J. Am. Chem. Soc.* **1997**, *119*, 7797−7806.
(45) Fischer, M. W. F.; Zeng, L.; Pang, Y. X.; Hu, W. D.; Majumdar, A.; Zuiderweg, E. R. P. *J. Am. Chem. Soc.* **1997**, *119*, 12629−12642.
(46) Tessari, M.; Vis, H.; Boelens, R.; Kaptein, R.; Vuister, G. W. *J. Am. Chem. Soc.* **1997**, *119*, 8985−8990.
(47) Tjandra, N.; Bax, A. *J. Am. Chem. Soc.* **1997**, *119*, 8076−8082.
(48) Kontaxis, G.; Clore, G. M.; Bax, A. *J. Magn. Reson.* **2000**, *143*, 184−196.

Here, we present measurements of the average magnitude and orientation of the $^{15}N$, $^{13}C'$, and $^{1}H^{N}$ chemical shift tensors in the protein ubiquitin, and their relation to secondary structure. Analogous to the earlier study of the $^{15}N$ CSA effect on the observed chemical shift in the magnetically aligned case,[39] these tensors can be measured from the change in chemical shift between the oriented and isotropic states. Relative to the case of magnetic alignment, the degree of macromolecular alignment is much increased by dissolving them in an aqueous, dilute liquid crystalline phase of large disc-shaped phospholipid particles. However, the degree of alignment in such a medium is kept sufficiently small that the NMR spectrum retains the simplicity and high-resolution appearance of the regular solution.[50] This approach has previously been used for studies of both the $^{13}C'$ and $^{15}N$ CSA tensors.[40,51] The phospholipid particles, commonly referred to as bicelles,[52−54] consist of a mixture of dimyristoyl-phosphatidylcholine (DMPC) and dihexanoyl-phosphatidylcholine (DHPC).[52] These bicelles are planar, disc-shaped particles with the DMPC making up the plane of the disk and the detergent DHPC covering the rim. Model calculations suggest that, depending on the DMPC:DHPC molar ratio and their volume fraction in water, the bicelles are 400−800 Å in diameter.[52,53,55,56] Just above room temperature, the particles form a nematic liquid crystalline suspension and align cooperatively with the magnetic field, with an ordering parameter of ca. 0.65. The liquid crystalline phase can be retained down to phospholipid volume fractions as low as 3%,[52,57] and the rotational diffusion rate of the macromolecular solute in the large aqueous spaces separating individual bicelles is not measurably affected by the bicelles.[57] The degree of molecular alignment of the solute protein in such a system is weak, on the order of $10^{-3}$, and consequently the changes in chemical shifts between aligned and isotropic phases span a range which is 3 orders of magnitude smaller than the width of the corresponding CSA powder pattern observed in the solid state. Because of the high precision at which the protein resonance frequencies in the liquid crystalline and isotropic solution states can be measured, these small chemical shift changes nevertheless can be determined at very high accuracy and be correlated with the magnitude and orientation of the corresponding CSA tensors.

The degree of alignment of the protein is determined from the $^{1}H-^{15}N$ one-bond dipolar couplings. The ratios of the $^{1}H-^{15}N$ and $^{13}C-^{15}N$ dipolar couplings indicate an effective N−H bond length of 1.04 Å if the C′−N distance is assumed to be equal to the crystallographically determined value of 1.33 Å.[58] This 1.04 Å value is 0.02 Å longer than commonly used in NMR relaxation studies, but accounts for the larger amplitude librations of the N−H vector relative to the C′−N vector. Assuming that motions of the backbone scale the effective CSA and the $^{13}C-^{15}N$ dipolar interactions by the same factor, use of a 1.04 Å N−H reference distance results in CSA values for a protein in the absence of internal backbone (C′−N) motion.

Motions in a cone scale down the changes in chemical shift and the observed dipolar couplings by the same factor $S$,[59] and therefore have no effect on the derived average CSA values. $S$ is the square root of the generalized order parameter commonly used in NMR relaxation studies. Considering that $S^2$ is rather uniform along the polypeptide backbone, the deviation from the average scale factor is quite small. An attempt to account for the degree of motion, previously reported for the backbone $^{15}N$ sites in ubiquitin, did not yield a significant improvement in the fit of the data.

Throughout this paper we report the values of the chemical shielding tensor, $\sigma$, which by convention has the opposite sign of the chemical shift tensor.

## Experimental Section

Spectra for ubiquitin were recorded for a sample containing 0.7 mM protein uniformly enriched in $^{2}H$, $^{13}C$, and $^{15}N$, dissolved in a medium containing 50 mg/mL of phospholipid bicelles, consisting of a 1:30:10 molar ratio of cetyltrimethylammonium bromide (CTAB),[60] dimyristoyl-phosphatidylcholine (DMPC), and dihexanoyl-phosphatidylcholine (DHPC), prepared as described previously.[56] The solvent consists of 93% $H_2O$, 7% $D_2O$, 10 mM phosphate buffer, pH 6.6, and 0.15 mM sodium azide. The sample was contained in a 240 $\mu$L Shigemi microcell. All data were recorded at 600 MHz $^{1}H$ frequency, using a Bruker DMX-600 spectrometer.

$^{1}H^{N}$, $^{15}N$, and $^{13}C'$ chemical shifts and $D_{NH}$ dipolar couplings were measured from a single 3D HNCO experiment,[61] modified in the standard manner by the addition of pulsed field gradients (Figure 1).[62,63] Spectra were acquired at 600 MHz $^{1}H$ frequency, as 80*($t_1$, $^{15}N$) × 100*($t_2$, $^{13}C$) × 768*($t_3$, $^{1}H$) data matrices, with 2 scans per hypercomplex ($t_1$, $t_2$) pair, at four temperatures: 12, 17, 24, and 31 °C. Acquisition times were 160 ms in the $t_3$ dimension, 100 ms in the $t_1$ dimension, and 110 ms in the $t_2$ dimension. The total measuring time was approximately 43 h per spectrum. Apodization with 72°-shifted ($t_3$, $t_2$) and 90°-shifted ($t_1$) sine bell filters was used prior to extensive zero filling to yield a digital resolution of 2.3 ($^{1}H$), 1.6 ($^{15}N$), and 1.8 Hz ($^{13}C'$) in the final spectra. $^{1}H^{N}-^{15}N$ dipolar couplings were derived from the change in $F_1$ splittings, recorded in the liquid crystalline (31 °C) and isotropic (17 °C) states. Data were processed and peak picked using the NMRPipe software package.[64]

## Results and Discussion

**Measurement of $D_{NH}$ and $\Delta\delta$.** In previous studies by us[51] and by Boyd and Redfield[40] the change in $^{13}C'$ and $^{15}N$ chemical shift, $\Delta\delta$, between isotropic and aligned phases was measured and compared with values predicted from the molecular structure. Studying hen lysozyme, Boyd and Redfield found a −173 ppm value for the backbone $^{15}N$ CSA. Our data for $^{13}C'$ were compatible with CSA data derived from solid-state measurements, but no explicit attempt was made to optimize the fit by adjusting the $^{13}C'$ CSA tensor values used. When searching for CSA values which optimize the fit between observed $\Delta\delta$ values and those predicted by the structure and its alignment tensor, derived from one-bond dipolar couplings, it is critical to ensure that the degree of molecular alignment is the same when measuring the dipolar couplings and when recording the chemical shifts. For example, a small increase in

(49) Gerald, R.; Bernhard, T.; Haeberlen, U.; Rendell, J.; Opella, S. *J. Am. Chem. Soc.* **1993**, *115*, 777−782.
(50) Tjandra, N.; Bax, A. *Science* **1997**, *278*, 1111−1114.
(51) Cornilescu, G.; Marquardt, J. L.; Ottiger, M.; Bax, A. *J. Am. Chem. Soc.* **1998**, *120*, 6836−6837.
(52) Sanders, C. R.; Schwonek, J. P. *Biochemistry* **1992**, *31*, 8898−8905.
(53) Sanders, C. R.; Hare, B. J.; Howard, K. P.; Prestegard, J. H. *Prog. Nucl. Magn. Reson. Spectrosc.* **1994**, *26*, 421−444.
(54) Salvatore, B. A.; Ghose, R.; Prestegard, J. H. *J. Am. Chem. Soc.* **1996**, *118*, 4001−4008.
(55) Vold, R. R.; Prosser, R. S. *J. Magn. Reson. Ser. B* **1996**, *113*, 267−271.
(56) Ottiger, M.; Bax, A. *J. Biomol. NMR* **1998**, *12*, 361−372.
(57) Bax, A.; Tjandra, N. *J. Biomol. NMR* **1997**, *10*, 289−292.
(58) Ottiger, M.; Bax, A. *J. Am. Chem. Soc.* **1998**, *120*, 12334−12341.
(59) Fischer, M. W. F.; Losonczi, J. A.; Weaver, J. L.; Prestegard, J. H. *Biochemistry* **1999**, *38*, 9013−9022.
(60) Losonczi, J. A.; Prestegard, J. H. *J. Biomol. NMR* **1998**, *12*, 447−451.
(61) Kay, L. E.; Ikura, M.; Tschudin, R.; Bax, A. *J. Magn. Reson.* **1990**, *89*, 496−514.
(62) Bax, A.; Pochapsky, S. S. *J. Magn. Reson.* **1992**, *99*, 638−643.
(63) Kay, L. E.; Keifer, P.; Saarinen, T. *J. Am. Chem. Soc.* **1992**, *114*, 10663−10665.
(64) Delaglio, F.; Grzesiek, S.; Vuister, G. W.; Zhu, G.; Pfeifer, J.; Bax, A. *J. Biomol. NMR* **1995**, *6*, 277−293.

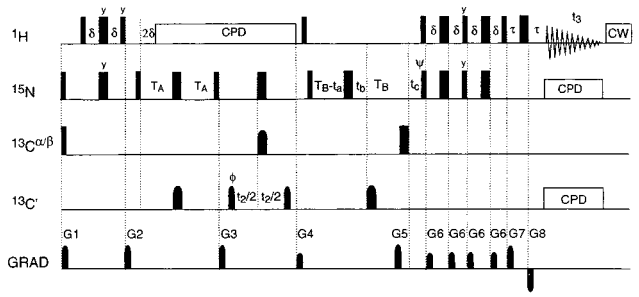


**Figure 1.** Pulse scheme of the 3D HNCO experiment, used to measure $^1H^N$, $^{15}N$, and $^{13}C'$ chemical shifts and $D_{NH}$ dipolar couplings. Narrow and wide pulses correspond to flip angles of 90° and 180°, respectively. All pulse phases are *x*, unless specified. $^{13}C'$ pulses have the shape of the center lobe of a sin(*x*)/*x* function, and durations of 170 $\mu$s. $^{13}C'$ pulses bracketing the $t_1$ evolution period are 90° and the other two $^{13}C'$ pulses are applied at four times higher power and correspond to 180°. Composite pulse decoupling (WALTZ16) was used on all three channels. To minimize the effect of radio frequency heating during $^{13}C'$ evolution period, a temperature-compensating CW irradiation (200 kHz off-resonance) period is used, which is decreased when $t_2$ is increased, such that the total amount of heat generated per scan remains independent of $t_2$.[82] The $^{13}C^{\alpha/\beta}$ pulse during $^{13}C'$ evolution is a 500 $\mu$s hyperbolic secant pulse.[83] Delay durations: $\delta = 2.65$ ms, $\tau = 0.25$ ms, $T_A = 12.5$, $T_B = 16$ ms. Evolution period $t_1$ ($^{15}N$) takes place during the interval $2T_B - t_a + t_b + t_c$ and is of the mixed-constant-time variety.[84,85] Using $N$ $t_1$ increments, the $t_a$, $t_b$, and $t_c$ increments are given by $\Delta t_a = T_B/N$; $\Delta t_c = T_{max}/2N$, where $T_{max}$ is the total duration of the last $t_1$ increment, and $\Delta t_b = \Delta t_c - \Delta t_a$, and initial durations (first $t_1$ increment) $t_a = t_b = t_c = 0$. Phase cycling: $\phi = x, -x$. Receiver = $x, -x$. Rance−Kay coherence selection was used in the $t_1$ dimension, with data stored separately for $\psi = -x$ and positive polarity for gradient G5, and $\psi = x$ for negative polarity.[61] Pulsed field gradients are sine-bell shaped with (strength in G/cm, duration in ms, axes): G1 (25, 0.4, *x*/*y*), G2 (25, 1.1, *y*), G3 (25, 0.7, *y*/*z*), G4 (15, 1.3, *y*), G5 (±25, 2.705, *z*), G6 (15, 1.0, *x*), G7 (25, 0.2, *z*), G8 (−25, 0.0756, *z*).

temperature during the measurement of dipolar couplings would increase the derived molecular alignment (without measurably changing the tensor orientation).[56] If chemical shifts were measured at slightly lower temperature (with weaker alignment) the derived best-fit CSA values would underestimate the true values. Therefore, it is critical that the conditions under which the dipolar couplings are measured are the same as those used for chemical shift measurements. This requirement is automatically satisfied when the shifts and couplings are derived from the same data set. As we aim to measure $^1H^N$, $^{15}N$, and $^{13}C'$ CSA tensors, the experiment was designed to measure all three shifts and the dipolar couplings simultaneously, from a single 3D experiment.

The 3D HNCO experiment used for collecting the $^1H^N-^{15}N$ dipolar couplings and $^1H^N$, $^{15}N$, and $^{13}C'$ is shown in Figure 1. It is in essence identical to the cpd-HNCO experiment,[65] supplemented by gradient enhanced transfer of magnetization from $^{15}N$ to $^1H^N$.[63] $^1H$ decoupling is omitted during the mixed-constant-time $^{15}N$ evolution period, and an antiphase $^{15}N-\{^1H^N\}$ doublet is obtained in this dimension. The experiment is recorded with long acquisition times in all three frequency dimensions and yields a rather large data matrix (2 GB) for the absorptive component of the final 3D spectrum, despite extensive use of aliasing in the $^{13}C'$ and $^{15}N$ dimensions.

Figure 2A shows a superposition of small regions taken from ($F_1$,$F_3$) cross sections of the three 3D spectra recorded at 17, 24, and 31 °C. The cross sections are taken at a $^{13}C'$ frequency

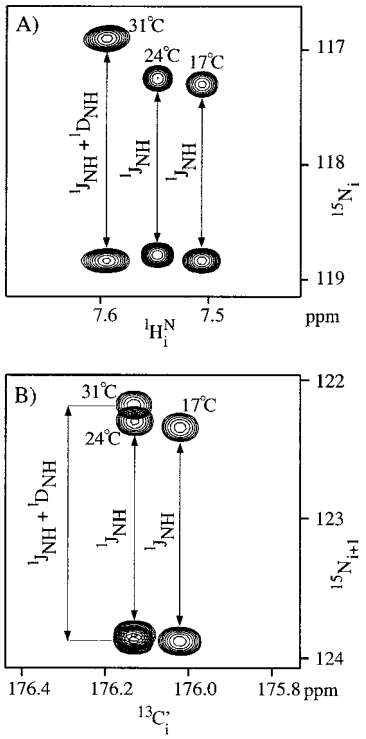


**Figure 2.** Overlay of the $^1H-^{15}N$ and $^{15}N-^{13}C'$ doublet components of residue Gln$^{41}$ ($i = 41$) taken from the 600 MHz 3D HNCO spectrum of uniformly $^{13}C/^{15}N/^2H$-enriched human ubiquitin (0.7 mM) in 93% $H_2O$, 7% $D_2O$, pH 6.6, containing 5% w/v bicelles, with a 30:10:1 molar ratio of DMPC:DHPC:CTAB. The superimposed cross sections are taken from spectra recorded at 17, 24, and 31 °C.

of about 176 ppm, and show the $^{15}N-\{^1H^N\}$ doublets of Gln$^{41}$. As can be seen from this spectrum, each doublet yields two independent measurements of the $^1H^N$ chemical shift, provided $^{13}C'$ decoupling is used during $t_3$.[66,67] Similarly, cross sections orthogonal to the $^1H^N$ axis (Figure 2B) show that the doublet also yields two independent measurements for the $^{13}C'$ chemical shift. The random uncertainty in the averaged $^1H^N$ resonance frequency equals half the pairwise root-mean-square difference (rmsd) in chemical shift between the downfield and upfield doublet components (0.05 ppb for the isotropic spectra, 0.11 ppb for the spectra in the liquid crystalline phase). Similarly, the estimated random error in the averaged $^{13}C'$ chemical shift is 0.16 ppb (the same for all three 3D spectra). The $^{15}N$ chemical shift corresponds to the average of the frequencies of the two doublet components, but as the peak positions occur at $\delta_N \pm J_{NH}/2$ the uncertainty in the average is $\sqrt{2}$ larger than the uncertainty in the $^{15}N$ frequency of an individual doublet component. Considering the line width (in hertz) is very similar in the $^{13}C'$ and $^{15}N$ dimensions, the $^{15}N$ chemical shift uncertainty in hertz is estimated to be 2-fold larger, i.e., 0.8 ppb.

The $^1H^N$, $^{15}N$, and $^{13}C'$ chemical shifts measured at 17, 24, and 31 °C are listed in the Supporting Information. Data at a fourth temperature (12 °C) were recorded to investigate the linearity of the chemical shift dependence on temperature. Only for $^1H^N$ was this nonlinear behavior noticible (see below).

**NMR Structure of Ubiquitin.** Initially, the measured $\Delta\delta$ data were correlated with the previously determined NMR

(65) Grzesiek, S.; Bax, A. *J. Magn. Reson.* **1992**, *96*, 432−440.

(66) Wang, Y. X.; Jacob, J.; Cordier, F.; Wingfield, P.; Stahl, S. J.; Lee-Huang, S.; Torchia, D.; Grzesiek, S.; Bax, A. *J. Biomol. NMR* **1999**, *14*, 181−184.

(67) Yang, D. W.; Kay, L. E. *J. Biomol. NMR* **1999**, *14*, 273−276.

structure (PDB identifier 1D3Z),[51] which was calculated on the basis of 27 H-bond, 754 dipolar, 2727 NOE, and 98 dihedral angle restraints, derived from homo- and heteronuclear *J* couplings. Although the fit between $\Delta\delta$ data and this structure was considerably better than to the X-ray structure[68] (which differs from the NMR structure by a rmsd of 0.35 Å for the backbone atoms), the value for the $^{13}C'$ CSA obtained when using this structure was 5% larger than that obtained from the crystal structure, whereas fitted values for the $^{1}H^{N}$ and $^{15}N$ CSA tensor differed by less than 2%. The reason for this $^{13}C'$ CSA discrepancy appears to be rather subtle and is related to the nonuniformity of the distribution of the $^{13}C'$ CSA principal axes with respect to the alignment tensor of ubiquitin. As the orientation of backbone peptide groups is primarily determined by the one-bond heteronuclear dipolar couplings ($^{1}D_{NH}$, $^{1}D_{C'C\alpha}$, $^{1}D_{C'N}$, and $^{1}D_{H\alpha C\alpha}$), small deviations from the effective bond lengths can cause a systematic twist of the peptide plane with respect to the alignment tensor. Previously, these effective bond lengths were derived from comparing measured dipolar couplings with the crystal structure of ubiquitin.[58] Using exactly the same set of input data, but changing the effective bond lengths in an extensive iterative scheme, we were able to find effective bond lengths which yielded NMR structures with significantly lower potential energy than obtained with these earlier values. The optimal ratios of the effective dipolar couplings relative to those for an N−H vector pointing in the same direction were found to be 2.08 ($C^{\alpha}-H^{\alpha}$), 0.198 ($C^{\alpha}-C'$), 0.120 ($C'-N$), and 0.300 ($C'-H^{N}$). This corresponds to a shortening of the effective $C^{\alpha}-H^{\alpha}$ bond by 0.01 Å, and a lengthening of the $C'-H^{N}$ distance by 0.035 Å relative to the values used[58] in the original NMR structure calculation, the other bond lengths remaining virtually unchanged. Although use of these adjusted effective bond lengths considerably improves the fit between the experimental dipolar couplings and the calculated NMR structure, the change in the backbone atom positions relative to the earlier structure (PDB identifier 1D3Z) is extremely small (0.07 Å for the backbone atoms).

**Determination of the Alignment Tensor.** The measured $\Delta\delta$ ubiquitin data were correlated both with its 1.8 Å X-ray structure[68] and with the NMR structure, recalculated in the manner described above. Proton positions were added to the crystal structure using the program XPLOR,[69] with $^{1}H^{N}$ in the $C'_{i-1}-N_i-C^{\alpha}_i$ plane, and the $C'_{i-1}-N_i-H^{N}_i$ angle equal to the $H^{N}_i-N_i-C^{\alpha}_i$ angle.

Experimental dipolar couplings were derived from the difference in $^{15}N-\{^{1}H^{N}\}$ splitting measured at 31 and 17 °C. These values are listed in the Supporting Information. $J_{NH}$ splittings measured at 24, 17, and 12 °C are indistinguishable from one another within experimental uncertainty. However, parenthetically we note that at 25 °C small dipolar contributions are present, which are approximately 15-fold smaller than those measured at 31 °C (data not shown). This suggests that right at the temperature where the DMPC alkane chains melt from an all-trans crystalline conformation to a gel phase, a very small degree of protein alignment already occurs, even though no quadrupolar splitting of the $^{2}H$ lock signal is visible. Presumably this is related to transient formation of microscopically small domains of bicelles, ordered in a nematic liquid crystalline manner. At temperatures higher than 25 °C but lower than 28 °C, the sample is unstable, however, and separates into an ordered liquid crystalline phase below an isotropic phase.[56]

**Table 1.** Alignment Tensor Orientation and Magnitude of Ubiquitin in the Liquid Crystalline Phase[a]

| structure | α | $\beta$ | $\gamma$ | $10^4A_{zz}$ | $10^4A_{yy}$ | $10^4A_{xx}$ |
|---|---|---|---|---|---|---|
| NMR[b] | 29° | 31° | 22° | 8.0 | −7.7 | −0.4 |
| X-ray | 27° | 31° | 23° | 8.0 | −7.5 | −0.5 |

[a] Using 5% w/v bicelles in 93% $H_2O$, 7% $D_2O$ at 31 °C. The Euler angles α, $\beta$, and $\gamma$ define the alignment tensor relative to the coordinate frame of the 1.8 Å X-ray structure[66] (using the convention of successive rotations around the *z*, *y*, *z* axes). The NMR structure was oriented to yield a best fit to the $C^{\alpha}$ atoms of the 1.8 Å X-ray structure prior to calculating the alignment tensor. [b] Calculated using 2727 NOEs, 27 H-bond, 754 dipolar, and 98 dihedral angle restraints derived from homo- and heteronuclear *J* couplings.

The dipolar coupling between two nuclei, A and B, in a solute macromolecule of fixed shape is related to the traceless alignment tensor according to:

$$D_{AB} = \sum_{i=x,y,z} -(\mu_0 h/8\pi^3)\gamma_A\gamma_B\langle r_{AB}^{-3}\rangle \cos^2\phi_i A_{ii} \qquad (1)$$

where $\phi_i$ is the angle between the A−B bond vector and the $A_{ii}$ principal axis of the alignment tensor, $\gamma_A$ and $\gamma_B$ are the gyromagnetic ratios of the two nuclei, and $\langle r_{AB}^{-3}\rangle$ is the vibrationally averaged inverse cube of the distance between the two nuclei. The orientation and magnitude of the rhombic alignment tensor were obtained from fits of the dipolar coupling data to the ubiquitin X-ray and NMR structures, using in-house written software.[70] Plots of the correlations between the experimental $D_{NH}$ values and the best-fitted values are presented in the Supporting Information.

The best-fit alignment tensor values are presented in Table 1. These values are based on the vibrationally corrected N−H bond length of 1.04 Å.[58] Simulations showed that experimental errors in the measurement of the dipolar couplings, which have a root-mean-square amplitude of 0.1 Hz, have a negligible effect on the derived value of **A**. Instead, random uncertainties in the magnitude and orientation of **A** are dominated by the uncertainties in (a) the X-ray and NMR ubiquitin structures, (b) the model-built positions of the amide protons relative to the peptide bond in the X-ray structure, and (c) the invalidity of the rigid body assumption.[58]

**Measurement of CSA Contribution to Chemical Shift.** The change in chemical shift for a given atom upon switching from the isotropic to the liquid crystalline phase is given by:

$$\Delta\delta = \sum_{i=x,y,z}\sum_{j=x,y,z} A_{jj}\cos^2\theta_{ij}\delta_{ii} \qquad (2)$$

where $\theta_{ij}$ is the angle between the $\delta_{ii}$ principal axis of the traceless CSA tensor and the $A_{jj}$ principal axis of the diagonalized traceless molecular alignment tensor, determined from the dipolar couplings in the manner described above.

As $\Delta\delta$ values are extremely small, it is generally not possible to accurately measure them directly from the difference in chemical shift in an isotropic sample and in a liquid crystalline sample. Chemical shifts are known to be extremely sensitive to experimental conditions, pH, and ionic strength in particular, and in practice it is not possible to prepare a bicelle-containing protein sample and a regular sample which differ by less than 1 part per billion (ppb) in chemical shift for $^{1}H^{N}$, $^{15}N$, and $^{13}C'$. In contrast, the temperature dependence of the chemical shift is small and relatively constant over a wide range of temperature. It is critical, however, that the spectra are carefully phased to

(68) Vijay-Kumar, S.; Bugg, C. E.; Cook, W. J. *J. Mol. Biol.* **1987**, *194*, 531−544.

(69) Brunger, A. T. *XPLOR Manual Version 3.1*; Yale University: New Haven, CT, 1993.

(70) Tjandra, N.; Grzesiek, S.; Bax, A. *J. Am. Chem. Soc.* **1996**, *118*, 6264−6272.

be purely absorptive, as even small changes in phase can alter the measured position of a resonance significantly, approximately by $(3.2 \times 10^{-3})$LW per degree phase error, where LW is the applicable line width at half-height.[48] This phasing requirement is frequently more difficult to meet in the directly detected dimension of a 3D NMR spectrum than in the indirectly detected dimensions, where the required phasing parameters are easily calculated in advance and do not require iterative adjustment.[71]

We derived the CSA contribution, $\Delta\delta$, to the chemical shift by measuring the chemical shifts in the aligned phase at 31 °C, and in the isotropic phase at 24 °C. The effect of the change in temperature on the chemical shift can be corrected for either by measuring its magnitude for a sample without bicelles or by measuring the shifts at two temperatures in the isotropic phase (17 and 24 °C), and assuming that the chemical shift has a linear dependence on temperature over the entire range of 17−31 °C. Here, this latter approach was used:

$$\Delta\delta_X = \delta_X(31\ ^\circ\mathrm{C}) - 2\delta_X(24\ ^\circ\mathrm{C}) + \delta_X(17\ ^\circ\mathrm{C}) \qquad (3)$$

where X is $^{13}C'$ or $^{15}N$, and $\delta_X$ is the chemical shift of X. For the $^1H^N$ chemical shifts, the anisotropic contribution to the chemical shift tends to be considerably smaller than the effect of changes in temperature. For $^1H^N$ therefore, a quadratic temperature dependence assumption was tested, which resulted in a better correlation between observed and predicted $\Delta\delta_H$ values. To obtain the second-order temperature coefficient, an additional spectrum was recorded at 12 °C, and the following linear system was solved for $\alpha$ and $\beta$ to obtain $\Delta\delta_H$.

$$\delta_H(12\ ^\circ\mathrm{C}) = -12\kappa\alpha + 144\kappa^2\beta + \delta_H(24\ ^\circ\mathrm{C}) \qquad (4a)$$

$$\delta_H(17\ ^\circ\mathrm{C}) = -7\alpha + 49\beta + \delta_H(24\ ^\circ\mathrm{C}) \qquad (4b)$$

$$\Delta\delta_H = \delta_H(31\ ^\circ\mathrm{C}) - \delta_H(24\ ^\circ\mathrm{C}) - (7\alpha + 49\beta) \qquad (4c)$$

where $\alpha$ and $\beta$ are the residue-specific linear and quadratic temperature coefficients, and the temperature dependence of $\delta_H$ is a parabola passing through the origin arbitrarily chosen at 24 °C. The global parameter $\kappa$ corrects for small deviations from linearity in the temperature setting, and is selected such that the mean square value of the quadratic temperature factors $(1/N)\sum_{i=1}^{N}\beta_i^2$ is minimized, where the summation extends over all $N$ residues in the structured region of the protein for which $\delta_H$ values were obtained. Residue specific $\Delta\delta$ values for $^{13}C'$ or $^{15}N$ and $^1H^N$ and temperature factors, $\alpha$ and $\beta$, are listed in the Supporting Information.

Knowing the magnitude and orientation of the molecular alignment tensor, and assuming uniform $^{13}C'$, $^{15}N$, and $^1H^N$ CSA tensors, residue specific $\Delta\delta$ values can be predicted by using eq 2. Previously, a quality factor, $Q$, was introduced to evaluate the agreement between the predicted and observed $\Delta\delta$ values:

$$Q = \mathrm{rms}(\Delta\delta^{\mathrm{meas}} - \Delta\delta^{\mathrm{pred}})/\mathrm{rms}(\Delta\delta^{\mathrm{meas}}) \qquad (5)$$

where $\Delta\delta^{\mathrm{pred}}$ is obtained after best fitting the measured data to the structure, using an optimized uniform CSA value obtained from a grid search procedure. A similar equation can be used for dipolar couplings.[72] Clearly, $Q$ is directly related to Pearson's linear correlation factor, $R$ (Figure 3). As can be seen from Figure 3, for the high degree of correlation typically obtained between measured data and high-quality structures ($R > 0.95$), $Q$ is a more convenient parameter for assessing the quality of such highly correlated data.

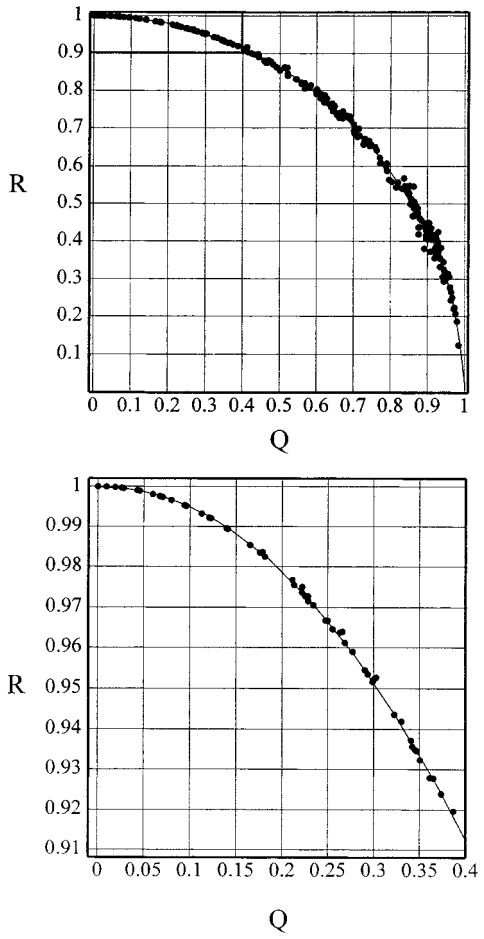


**Figure 3.** Relation between the quality factor $Q$ (eq 5 in text) and Pearson's linear correlation factor, $R$. The graphs (top, full graph; bottom, expansion) were generated by starting with the ubiquitin structure and calculating predicted $\Delta\delta_{C'}$ values ($\Delta\delta_{C'}^{\mathrm{pred}}$) using the CSA parameters in the top line of Table 2 and the alignment tensor of Table 1. Subsequently, $\Delta\delta_{C'}^{\mathrm{pred,noise}}$ sets are generated by adding random noise to $\Delta\delta_{C'}^{\mathrm{pred}}$, and $Q$ and $R$ factors are calculated for the $\Delta\delta_{C'}^{\mathrm{pred,noise}}$ versus $\Delta\delta_{C'}^{\mathrm{pred}}$ correlations.

A summary of the optimized CSA tensor values for $^{13}C'$, $^{15}N$, and $^1H^N$, together with the respective $Q$ factors for the correlations, is presented in Tables 2−4. The correlations between $\Delta\delta^{\mathrm{meas}}$ and $\Delta\delta^{\mathrm{pred}}$ are shown in Figures 4−6. Before discussing the relation between these CSA values and secondary structure, and before making comparisons with literature data, we first evaluate the estimated random errors in the CSA values derived in the above-described manner.

**Uncertainty in Average CSA.** The propagated experimental errors in the measured $\Delta\delta$, calculated using the precision estimated above for the individual chemical shifts, were 0.14 ppb for $^1H^N$, 1.6 ppb for $^{15}N$, and 0.3 ppb for $^{13}C'$. In all three cases, these random measurement errors are very much smaller than the rmsd between measured and predicted $\Delta\delta$ values (Tables 2−4). This indicates that the quality of the correlation is not significantly affected by the random error in measured $\Delta\delta$ values. Thus, there remain three sources that could significantly affect the correlations: errors in the atomic coordinates, intrinsic variations in the CSA tensor between the different sites, and invalidity of the assumption of uniform internal dynamics along the protein backbone. The fact that the

(71) Bax, A.; Ikura, M.; Kay, L. E.; Zhu, G. *J. Magn. Reson.* **1991**, *91*, 174−178.

(72) Ottiger, M.; Bax, A. *J. Biomol. NMR* **1999**, *13*, 187−191.

**Table 2.** Average $^{13}C'$ CSA Tensor Magnitude and Orientation in Ubiquitin

| structure | res. used | $\Delta\sigma^a$ (ppm) | $\eta^b$ | $\sigma_{11}$ (ppm) | $\sigma_{22}$ (ppm) | $\sigma_{33}$ (ppm) | $\beta$ (deg) | $Q$ (%) | rmsd[c] (ppb) | var.[d] (ppm) |
|---|---|---|---|---|---|---|---|---|---|---|
| NMR | all (64/62[e]) | 129.8 ± 3 (2[e]) | 0.73 | −74.7 ± 2 (1[e]) | −11.8 ± 3 (2[e]) | 86.5 ± 2 (1[e]) | 38 ± 2 (1[e]) | 14 (11[e]) | 9.9 (7.5[e]) | 13.3 (10.0[e]) |
| | helix (16) | 141.7 ± 3 | 0.51 | −71.2 ± 2 | −23.3 ± 4 | 94.5 ± 2 | 42 ± 3 | 6 | 4.6 | |
| | sheet (29/28[f]) | 126.0 ± 6 (4[f]) | 0.82 | −76.5 ± 3 (2[f]) | −7.5 ± 5 (4[f]) | 84.0 ± 4 (3[f]) | 37 ± 3 (2[f]) | 15 (12[f]) | 10.8 (8.2[f]) | |
| X-ray | all (64/62[e]) | 127.5 ± 4 | 0.72 | −73.3 ± 3 (2[e]) | −11.7 ± 4 (3[e]) | 85.0 ± 3 (3[e]) | 37 ± 3 (3[e]) | 21 (18[e]) | 14.6 (12.5[e]) | 19.1 (16.3[e]) |
| | helix (16) | 134.2 ± 9 | 0.56 | −69.9 ± 5 | −19.6 ± 10 | 89.5 ± 6 | 25 ± 10 | 16 | 12.5 | |
| | sheet (29/28[f]) | 124.4 ± 6 (4[f]) | 0.81 | −75.2 ± 4 (3[f]) | −7.7 ± 5 (4[f]) | 82.9 ± 4 (3[f]) | 37 ± 5 (4[f]) | 20 (15[f]) | 14.0 (10.8[f]) | |

[a] $\Delta\sigma = \sigma_{33} - (\sigma_{22} + \sigma_{11})/2$. [b] $\eta = |(\sigma_{int} - \sigma_{min})/\sigma_{max}|$, where the subscripts maximum (max), minimum (min), and intermediate (int) refer to the absolute magnitudes of $\sigma_{11}$, $\sigma_{22}$, and $\sigma_{33}$. [c] Pairwise rmsd between measured and best-fitted $\Delta\delta_{C'}$. [d] Estimated variability in the uniform CSA model (see section Variation in CSA Parameters). [e] Excluding residues Gly[10] and Val[70] (see Figure 4). [f] Excluding residue Val[70] (see Figure 4).

**Table 3.** Average Backbone $^{15}N$ CSA Tensor Magnitude and Orientation in Ubiquitin

| structure | res. used | $\Delta\sigma^a$ (ppm) | $\eta$ | $\sigma_{11}$ (ppm) | $\sigma_{22}$ (ppm) | $\sigma_{33}$ (ppm) | $\beta$ (deg) | $Q$ (%) | rmsd[b] (ppb) | var.[c] (ppm) |
|---|---|---|---|---|---|---|---|---|---|---|
| NMR | all (63) | −162.8 ± 4 | 0.16 | −108.5 ± 3 | 45.7 ± 2 | 62.8 ± 2 | 19 ± 1 | 17 | 10.5 | 12.7 |
| | helix (16) | −165.9 ± 9 | 0.09 | −110.6 ± 6 | 50.5 ± 5 | 60.1 ± 4 | 16 ± 2 | 21 | 9.8 | |
| | sheet (29) | −161.1 ± 6 | 0.24 | −107.4 ± 4 | 40.6 ± 3 | 66.8 ± 3 | 19 ± 1 | 17 | 10.6 | |
| X-ray | all (63) | −162.5 ± 4 | 0.19 | −108.4 ± 3 | 43.9 ± 2 | 64.5 ± 2 | 20 ± 1 | 20 | 12.5 | 15.1 |
| | helix (16) | −163.6 ± 9 | 0.07 | −109.0 ± 6 | 50.6 ± 4 | 58.4 ± 4 | 15 ± 3 | 25 | 11.5 | |
| | sheet (29) | −162.9 ± 6 | 0.27 | −108.6 ± 4 | 39.9 ± 3 | 68.7 ± 4 | 20 ± 1 | 21 | 12.7 | |

[a] $\Delta\sigma = \sigma_{11} - (\sigma_{22} + \sigma_{33})/2$. [b] Pairwise rmsd between best-fitted and observed $\Delta\delta_N$. [c] Estimated variability in the uniform CSA model.

**Table 4.** Average $^{1}H^N$ CSA Tensor Magnitude and Orientation in Ubiquitin

| structure | res. used | $\Delta\sigma^a$ (ppm) | $\eta$ | $\sigma_{11}$ (ppm) | $\sigma_{22}$ (ppm) | $\sigma_{33}$ (ppm) | $\beta$ (deg) | $Q$ (%) | rmsd[b] (ppb) | var.[c] (ppm) |
|---|---|---|---|---|---|---|---|---|---|---|
| NMR | all (64) | −8.9 ± 0.6 | 1.00 | −5.8 ± 0.3 | 0.0 ± 0.3 | 5.8 ± 0.4 | 8 ± 3 | 38 | 1.5 | 1.7 |
| | helix (16) | −7.2[d] ± 0.8 | 0.96 | −4.7 ± 0. 3 | 0.1 ± 0. 4 | 4.8 ± 0. 5 | 13 ± 9 | 36 | 1.1 | |
| | sheet (29) | −9.9 ± 0.8 | 1.00 | −6.6 ± 0.5 | 0.0 ± 0. 5 | 6.6 ± 0.6 | 7 ± 4 | 35 | 1.5 | |
| X-ray | all (64) | −8.7[d] ± 0.6 | 0.97 | −5.7 ± 0.4 | −0.1 ± 0.3 | 5.8 ± 0.4 | 8 ± 4 | 42 | 1.7 | 2.0 |
| | helix (16) | −7.0 ± 1.2 | 1.00 | −4.6 ± 0.6 | 0.0 ± 0.5 | 4.6 ± 0.8 | 8 ± 11 | 42 | 1.2 | |
| | sheet (29) | −9.8[d] ± 0.9 | 0.94 | −6.3 ± 0.5 | −0.2 ± 0.5 | 6.5 ± 0.6 | 10 ± 5 | 42 | 1.8 | |

[a] $\Delta\sigma = \sigma_{11} - (\sigma_{22} + \sigma_{33})/2$. [b] Pairwise rmsd between predicted and calculated $\Delta\delta_H$. [c] Estimated variability in the uniform CSA model (see section Variation in CSA Parameters). [d] For sign consistency, $\Delta\sigma$ is given as $\Delta\sigma = -(\sigma_{33} - (\sigma_{11} + \sigma_{22})/2)$.

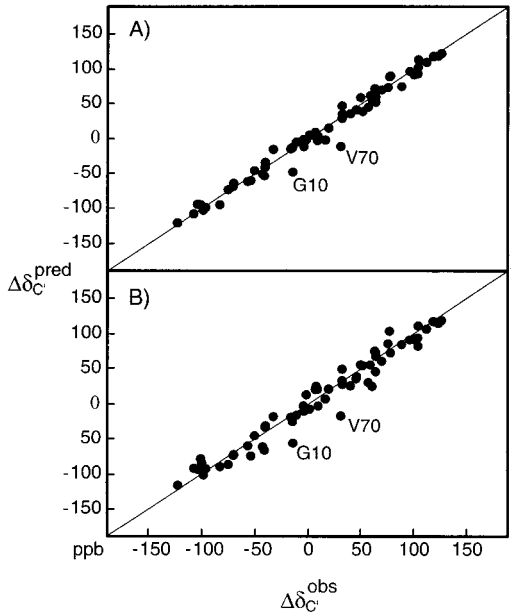


**Figure 4.** Correlations between observed $^{13}C'$ chemical shift changes, $\Delta\delta_{C'}^{obs}$, and $\Delta\delta_{C'}^{pred}$ values, predicted when using the CSA tensor values (Table 2) that provide the best fit between $\Delta\delta_{C'}^{obs}$ and $\Delta\delta_{C'}^{pred}$. (A) Correlation derived for the NMR structure and (B) for the 1.8 Å crystal structure of ubiquitin. Linear regression yields a correlation coefficient $R$ of 99.0% (99.5% without outliers Gly[10] and Val[70]) (A) and 97.8% (B).

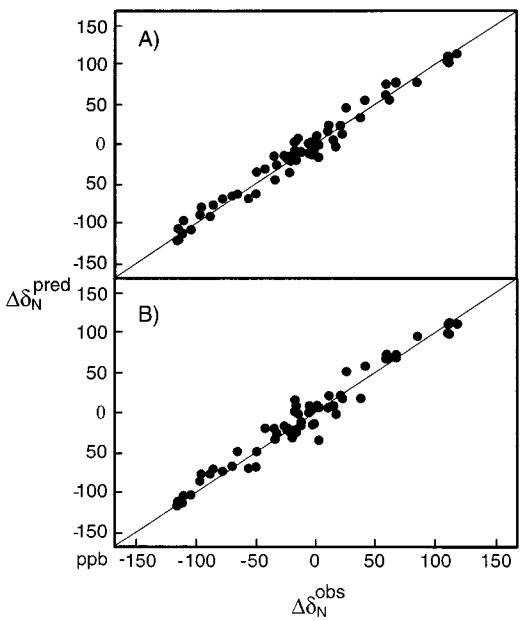


**Figure 5.** Correlations between observed $^{15}N$ chemical shift changes, $\Delta\delta_N^{obs}$, and $\Delta\delta_N^{pred}$ values, predicted when using the CSA tensor values (Table 3) that provide the best fit between $\Delta\delta_N^{obs}$ and $\Delta\delta_N^{pred}$. (A) Correlation derived for the NMR structure and (B) for the 1.8 Å crystal structure of ubiquitin. Linear regression yields correlation coefficients, $R$, of 98.6% for the NMR structure and 98.0% for the X-ray structure.

agreement between $\Delta\delta$ values and the NMR structure is considerably better than that with the X-ray structure (Tables 2−4 and Supporting Information) suggests that the residual scatter is dominated by uncertainty in the atomic coordinates, at least for the X-ray structure. Indeed, for ubiquitin X-ray structures solved at lower resolution[73,74] the agreement is considerably lower (data not shown). Variations in the order

(73) Cook, W. J.; Jeffrey, L. C.; Carson, M.; Chen, Z. J.; Pickart, C. M. *J. Biol. Chem.* **1992**, *267*, 16467−16471.
(74) Cook, W. J.; Jeffrey, L. C.; Kasperek, E.; Pickart, C. M. *J. Mol. Biol.* **1994**, *236*, 601−609.

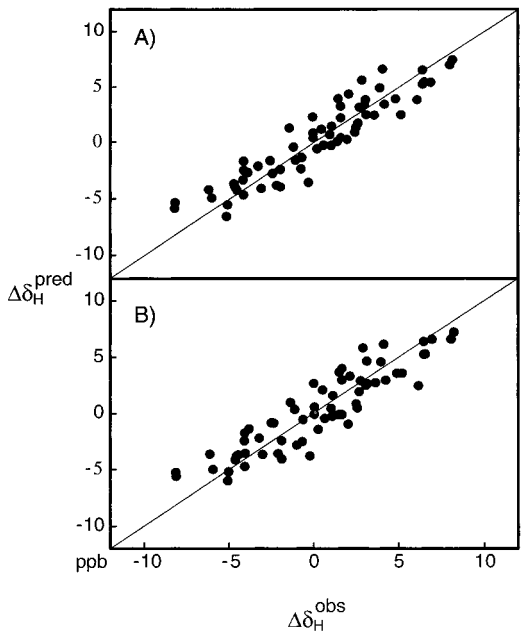


**Figure 6.** Correlations between observed $^1H^N$ chemical shift changes, $\Delta\delta_H{}^{obs}$, and $\Delta\delta_H{}^{pred}$ values, predicted when using the CSA tensor values (Table 4) that provide the best fit between $\Delta\delta_H{}^{obs}$ and $\Delta\delta_H{}^{pred}$. (A) Correlation derived for the NMR structure and (B) for the 1.8 Å crystal structure of ubiquitin. Linear regression yields correlation coefficients, *R*, of 92.5% for the NMR structure and 90.8% for the X-ray structure.

parameter *S* would result in differential scaling of the observed $\Delta\delta$ values. In this case, sites with the largest $\Delta\delta$ would be affected the most, which is the opposite of what is seen in Figure 4. Instead, uncertainty in the atomic coordinates results in the largest change in $\Delta\delta$ when the derivative is largest, i.e., when $\Delta\delta$ is relatively small. Therefore, this confirms that the uncertainty in the structure, and not the variation in *S*, is the main source of scatter in the correlation plots of Figures 4−6.

When comparing $^{13}C'$ $\Delta\delta_i{}^{pred} - \Delta\delta_i{}^{meas}$ values obtained with the 1.8 Å X-ray structure to those obtained for the NMR structure, the correlation is rather low ($R = 0.51$, when excluding outliers Gly[10] and Val[70]; Supporting Information). This indicates that uncertainty in the structure contributes significantly to the scatter in Figure 4. When comparing the $^{15}N$ $\Delta\delta_i{}^{pred} - \Delta\delta_i{}^{meas}$ values obtained with the X-ray structure with those obtained with the NMR structure, there is a somewhat stronger degree of correlation ($R = 0.64$, excluding outlier Glu[34], Supporting Information Figure 6B), indicating that intrinsic variations in the $^{15}N$ CSA also contribute significantly to the scatter in Figure 5. This type of correlation is even stronger for the $^1H^N$ case ($R = 0.92$, Supporting Information Figure 6C), indicating that the scatter in Figure 6 is dominated by variations in the $^1H^N$ CSA, and not by uncertainties in the atomic coordinates.

The scatter in the correlations in Figures 4−6 gives rise to uncertainty in the average value of the corresponding CSA, but no information on the error in the average orientation of the CSA tensor is derived in this manner. A different, Monte Carlo approach for assessing these errors therefore has been used. A total of 50 simulated $\Delta\delta^{noise}$ sets were generated by adding random Gaussian noise to the original set of $\Delta\delta^{pred}$ values, with the noise scaled to reproduce the same pairwise rmsd between $\Delta\delta^{noise}$ and $\Delta\delta^{pred}$ as had been found above, when optimizing the fit between $\Delta\delta^{meas}$ and $\Delta\delta^{pred}$. Re-fitting these Monte Carlo simulated data sets, $\Delta\delta^{noise}$, against the structure results in 50 new values for $\sigma_{11}$, $\sigma_{22}$, $\sigma_{33}$, and the angle $\beta$

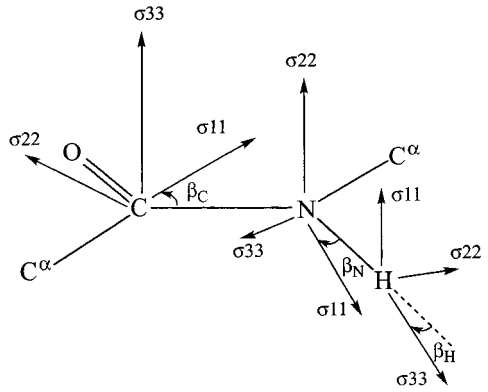


**Figure 7.** Orientation of the CSA tensor components $\sigma_{11}$, $\sigma_{22}$, and $\sigma_{33}$ relative to the peptide plane.

(defined in Figure 7). The standard deviations from the averages of these $\sigma_{11}$, $\sigma_{22}$, $\sigma_{33}$, and $\beta$ values then represent the uncertainties in the reported values (Tables 2−4).

**Variation in CSA Parameters.** As argued above, for $^{13}C'$ and to a lesser degree for $^{15}N$, the uncertainty in the structure contributes considerably to the scatter between $\Delta\delta^{meas}$ and $\Delta\delta^{pred}$, whereas for $^1H^N$ the scatter is dominated by intrinsic variations in the CSA tensor between the different protons. Nevertheless, if we assume that all scatter is dominated by intrinsic variations of the CSA tensor, upper limits for this degree of variation can be calculated in a manner very similar to the one described above for deriving the uncertainty in the average CSA tensor. For each residue, $\Delta\delta^{pred}$ values are calculated on the basis of the NMR structure and assuming for each residue the same, average $\sigma_{11}$, $\sigma_{22}$, $\sigma_{33}$, and $\beta$ values derived above. Then, Gaussian noise is added to each of the $\sigma_{11}$, $\sigma_{22}$, and $\sigma_{33}$ components (but not to $\beta$), with the noise added to different residues being uncorrelated, and the noise is scaled to reproduce the same scatter (*R* factor) between $\Delta\delta^{pred}$ and $\Delta\delta^{pred,noise}$ as observed in Figures 4−6. The standard deviation of the added noise provides an upper limit for the intrinsic variation in the CSA tensor components from one site to the next. A discussion of the average CSA values, their intrinsic scatter, and their dependence on secondary structure will be presented below for the three different types of nuclei, $^{13}C'$, $^{15}N$, and $^1H^N$.

**$^{13}C'$ CSA.** To a good approximation, peptide bonds are planar and therefore one of the principal components of the $^{13}C'$ CSA tensor is expected to be perpendicular to the peptide plane. Previous solid-state NMR studies on model peptides[25,26,28,30,75] have shown that it is the most shielded component, $\sigma_{33}$, that is approximately perpendicular to the peptide plane, causing $\sigma_{11}$ and $\sigma_{22}$ to lie in the peptide plane (throughout this paper we follow the convention $\sigma_{33} > \sigma_{22} > \sigma_{11}$). The orientation of the CSA tensor in the peptide coordinate system is then conveniently described by the angle between the least shielded component $\sigma_{11}$ and the C−N bond ($\beta_C$ in Figure 7). The orientations of the CSA tensors reported in these solid-state NMR studies agree quite well with one another, but the reported magnitudes vary considerably: The traceless components of the CSA tensor fall in the following ranges: $\sigma_{33}$ between 75 and 83 ppm; $\sigma_{22}$ between −13 ppm and +1 ppm; $\sigma_{11}$ between −77 ppm and −66 ppm, with $\beta_C$ between 35 and 47°.

The $^{13}C'$ CSA values obtained by fitting $\Delta\delta$ data against the NMR structure were $\sigma_{11} = -75 \pm 2$ ppm, $\sigma_{22} = -12 \pm 3$ ppm, and $\sigma_{33} = 87 \pm 2$ ppm, with an angle $\beta_C$ between the least shielded component $\sigma_{11}$ and the C′−N bond of 38 ± 2° (Table 2, Figure 7). These values correspond to an anisotropy

$\Delta\sigma = \sigma_{33} - (\sigma_{11} + \sigma_{22})/2$ of 130 ± 3 ppm, where the standard deviations are estimated using the above-described Monte Carlo method. A 2 ppm smaller CSA is found when relating the $\Delta\delta$ values to the crystal structure of ubiquitin. As noted above, when relating $\Delta\delta$ to the NMR structure, the fitted magnitude of the $^{13}C'$ CSA is relatively sensitive to the effective bond lengths used when calculating the structure. The 130 ppm $^{13}C'$ CSA is nearly 4 ppm smaller than the value obtained when using the original NMR structure as a reference, which was derived with slightly different scaling factors for the dipolar couplings, but may still contain a small systematic error.

A $\Delta\sigma$ value of 130 ppm is considerably larger than that found in most solid-state NMR studies, where experimental values range from 112 to 126 ppm. Interestingly, analyzing solution-state protein $^{13}C'$ relaxation data, Dayie and Wagner found a much wider range of $^{13}C'$ $\Delta\sigma$ values, which extended from about 120 to 160 ppm.[44] The same discrepancy was noted earlier between $^{15}N$ CSA values measured in the solid state and by solution relaxation studies, and has been attributed to the different ways in which motion is treated in the solution- and solid-state NMR experiments.[9,41,76,77] Considerable motion is present in the solid state, as judged, for example, by $^{15}N-^{13}C$ one-bond dipolar couplings, which are about 3−5% smaller than predicted on the basis of their crystallographically determined bond length.[25,75,78] In the present study, the molecular alignment tensor is indirectly referenced relative to a 1.33 Å C′−N bond length, resulting in a smaller alignment tensor and therefore larger CSA values than if the 1.34−1.35 Å solid-state NMR C′−N distance were used as a reference. So, in a comparison with the solid-state data, our CSA values need to be decreased by ∼3%, which puts them within the range of CSA values observed by solid-state NMR.

With an average angle $\beta_C$ (Figure 7) of 38°, the orientation of the $^{13}C'$ CSA tensor is very close to the average orientation observed in solid-state NMR studies. We also evaluated the validity of the assumption that, on average, the $\sigma_{33}$ axis is perfectly normal to the peptide plane. To this extent, a grid search was carried out, refitting the $\Delta\delta$ data for CSA tensors where the $\sigma_{33}$ axis is rotated in small steps around either the $\sigma_{11}$ or $\sigma_{22}$ axis (data not shown). A minute improvement in the fit was obtained when rotating $\sigma_{33}$ by 1.5° in a counterclockwise manner toward the $\sigma_{22}$ axis. However, the improvement in the fit was much too small to justify an additional degree of freedom, and therefore is not statistically significant. Hence, the $\Delta\delta$ data are in agreement with $\sigma_{33}$ oriented perpendicular to the peptide plane.

As shown in Figure 8A, when restricting the fitting procedure to residues in helical secondary structure, the NMR structure yields a very tight correlation with somewhat larger CSA values, $\Delta\sigma = 142 \pm 3$ ppm and reduced asymmetry, $\eta = |(\sigma_{int} - \sigma_{min})/\sigma_{max}| = 0.41$, where the subscripts maximum (max), minimum (min), and intermediate (int) refer to the absolute magnitudes of $\sigma_{11}$, $\sigma_{22}$, and $\sigma_{33}$. The increase in the helical $^{13}C'$ CSA is less pronounced for the crystal structure: $\Delta\sigma = 134 \pm 9$ ppm; $\eta = 0.46$ (Table 2). For sheet regions (Figure 8B), the fit yields $\Delta\sigma = 125 \pm 6$ ppm and $\eta = 0.75$, for both the NMR and X-ray structures. It is interesting to note that $\Delta\sigma$ is about 12 ppm larger for helical residues than for $\beta$-sheet and has

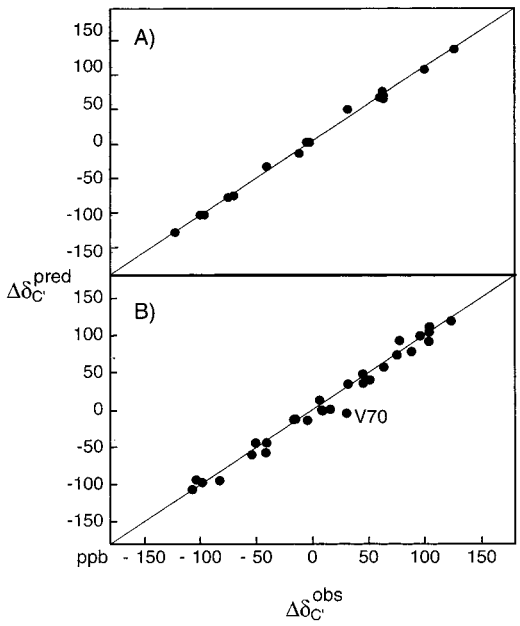


**Figure 8.** Correlations between observed $\Delta\delta_{C'}$ and best-fitted values are shown for (A) all helical residues (including the 3−10 helices) and (B) all $\beta$-sheet residues in the NMR structure of ubiquitin. Linear regression yields a correlation coefficient $R$ of 99.8% (A) and 98.9% (B).

considerably lower rhombicity. Remarkably, for the helical residues the orientation of the CSA principal axes ($\beta_C$) differs by 17° when using the X-ray and NMR structures (Table 2), and the uncertainty in the X-ray derived $\beta_C$ (±10°) is particularly large. The problem in determining accurate CSA orientations for the subset of helical residues is related to the fact that most of these residues are part of a single helix, which is nearly parallel to the $z$ axis of the molecular alignment tensor. In an α-helix, the $\sigma_{22}$ $^{13}C'$ CSA axis is also nearly parallel to the helix axis. Therefore, in ubiquitin most helical residues have their $\sigma_{22}$ axis nearly parallel to the $z$ axis of the molecular alignment tensor, and the distribution of helical $^{13}C'$ CSA tensors is highly nonuniform. Therefore, we believe the difference in $\beta_C$ between helix and sheet residues is not statistically significant. In contrast, the much smaller $\eta$ values in helix relative to sheet are pronounced and fall well outside the uncertainties in these parameters. The larger CSA and decreased rhombicity in helical regions agrees with recent solid-state NMR data, but contradicts theoretical calculations.[31]

When excluding outliers Gly[10] (mobile turn region)[79] and Val,[70] the quality factor, $Q$, of the correlation in Figure 4 is 10%, which is considerably better than that for $^{15}N$ and $^{1}H^{N}$ (Figures 5 and 6). Nevertheless, if the scatter in this correlation is all attributed to random, uncorrelated variations in the CSA tensor components of equal rms magnitude, a rather large upper limit of ±10 ppm is found for the rms amplitude of this variation. As mentioned before, the low degree of correlation between $\Delta\delta_i^{pred} - \Delta\delta_i^{meas}$ derived for the X-ray and NMR structure suggests that uncertainty in the atomic coordinates contributes considerably to the scatter in Figure 4, and thereby to the relatively large value of this ±10 ppm upper limit.

**$^{15}N$ CSA.** For convenience, in protein $^{15}N$ NMR relaxation studies the chemical shift tensor of backbone $^{15}N$ nuclei is

(75) Stark, R. E.; Jelinski, L. W.; Ruben, D. J.; Torchia, D. A.; Griffin, R. G. *J. Magn. Reson.* **1983**, *55*, 266−273.
(76) Tjandra, N.; Wingfield, P.; Stahl, S.; Bax, A. *J. Biomol. NMR* **1996**, *8*, 273−284.
(77) Ishii, Y.; Terao, T.; Hayashi, S. *J. Chem. Phys.* **1997**, *107*, 2760−2774.
(78) Harbison, G. S.; Jelinski, L. W.; Stark, R. E.; Torchia, D. A.; Herzfeld, J.; G., G. R. *J. Magn. Reson.* **1984**, *60*, 79−82.
(79) Tjandra, N.; Feller, S. E.; Pastor, R. W.; Bax, A. *J. Am. Chem. Soc.* **1995**, *117*, 12562−12566.

commonly assumed to be axially symmetric, with its unique axis located in the peptide plane and making a small angle, $\beta_N$, with the N−H bond vector,[27,28,30,33,78,80] i.e., nearly orthogonal to the peptide bond (Figure 7). Solid-state NMR measurements indicate considerable asymmetries of the $^{15}$N CSA tensor, however, with values for the traceless CSA tensor ranging from −115 to −95 ppm for $\sigma_{11}$, from 30 to 51 ppm for $\sigma_{22}$, and from 55 to 77 ppm for $\sigma_{33}$, and $\beta_N$ making an angle of 11−26° with the N−H bond. The asymmetry parameter, $\eta$, depends strongly on conformation, as exemplified most clearly in a study by Hiyama et al., who observed $\eta$ values of 0.06 and 0.44 for glycyl-glycyl-{$^{15}$ N}glycine in mono- and triclinic lattice forms.[33] The recent liquid crystal NMR study of lysozyme by Boyd and Redfield[40] also clearly indicates an average nonzero rhombicity, with shielding in the N−C′ direction ($\sigma_{33}$) about 17 ppm larger than orthogonal to the peptide plane ($\sigma_{22}$). Interestingly, both liquid crystal and solid-state NMR data suggest that the $\sigma_{33}$ component can rotate significantly out of the peptide plane.[40,43]

The fitting of $\Delta\delta$ values measured in this study against the NMR structure (Figure 5) yields $\Delta\sigma = -163 \pm 4$ ppm, $\eta = 0.14$, and an angle $\beta_N$ of 19° between the N−H bond and $\sigma_{11}$ (Table 3, Figure 7). The standard errors were estimated using the Monte Carlo procedure, described above. The correlation factor between $(\Delta\delta_i^{meas} - \Delta\delta_i^{pred,\ NMR})$ and $(\Delta\delta_i^{meas} - \Delta\delta_i^{pred,\ Xray})$ equals 0.64, indicating that the variation in the CSA tensor from one residue to the next is contributing somewhat more to the scatter in Figure 5 than it does for the $^{13}$C′ data of Figure 4.

The $^{15}$N CSA $\Delta\sigma$ value of $-163 \pm 3$ ppm again is based on a reference distance, $r_{NH}$, of 1.04 Å (corresponding to $r_{C'N} = 1.33$ Å). When using $r_{NH} = 1.02$ Å, a −173 ppm $\Delta\sigma$ value is obtained, which is in excellent agreement with the CSA value derived from $^{15}$N relaxation studies.[23,76] However, as argued above for $^{13}$C′, when comparing to solid-state data our CSA values need to be scaled down by ∼3%, yielding numbers very close to the average value observed by solid-state NMR.

Analogous to the $^{13}$C′ case described above, the dependence of the CSA tensor on secondary structure can be evaluated by restricting the fit to helical or $\beta$-sheet residues (Supporting Information, Figure 3). Results are summarized in Table 3. Interestingly, there is no significant change in the magnitude of the CSA tensor, but the average asymmetry in helical residues ($\eta = 0.06$) is considerably smaller than that in $\beta$-sheet ($\eta = 0.18$). This agrees with the increased rhombicity in extended conformations observed by solid-state NMR,[32] although their small decrease in the magnitude of $\Delta\sigma$ is not very pronounced in our data.

An upper limit for the intrinsic variation in $^{15}$N CSA can be estimated in the same manner as for $^{13}$C′, assuming again that all scatter in Figure 5 is caused exclusively by random, independent variations in $\sigma_{11}$, $\sigma_{22}$, and $\sigma_{33}$. This yields standard deviations of 12.7 ppm for the individual CSA components. As mentioned above, these standard deviations represent upper limits. However, considering that the correlation factor between $(\Delta\delta_i^{meas} - \Delta\delta_i^{pred,NMR})$ and $(\Delta\delta_i^{meas} - \Delta\delta_i^{pred,X-ray})$ equals 0.64, variations in the CSA tensor from one residue to the next indeed contribute considerably, and these standard deviations do not overestimate the intrinsic variation by a large amount. Random variation by 12.7 ppm in $\sigma_{nn}$ corresponds to a variation of 17 ppm in $\Delta\sigma$, which is somewhat larger than the ±9.6 ppm upper limit found by Kroenke et al. from field-dependent $^{15}$N relaxation studies.[23] Previously,[33,38] a tendency for $\sigma_{22}$ and $\sigma_{33}$ to vary in a correlated but opposite manner has been noted, however, which would lead to smaller variations in $\Delta\sigma$ than the 17 ppm upper limit derived above. The smaller upper limit of Kroenke et al. therefore is also compatible with correlated, opposite sign variations in $\sigma_{22}$ and $\sigma_{33}$.

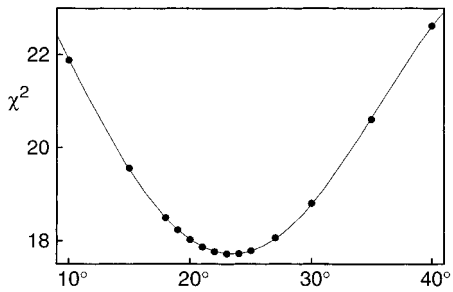


**Figure 9.** $\chi^2$ value for the best fit between experimental $\Delta\delta_N$ and the NMR structure, as a function of the rotation of $\sigma_{22}$ and $\sigma_{33}$ about the $\sigma_{11}$ vector (clockwise is positive, when viewed in the $\sigma_{11}$ direction) for all helical residues. The reduction in $\chi^2$ upon rotation is statistically significant ($P_F = 2\%$).

There appears to be a small difference between α-helix and $\beta$-sheet in the average orientation of the $^{15}$N CSA tensor, as judged by the angle $\beta_N$, with slightly (∼4°) smaller values in helical residues than in sheet.

We also evaluated the correctness of the assumption that $\sigma_{22}$ is orthogonal to the peptide plane. As for $^{13}$C′, a grid search was conducted in which the $\Delta\delta$ data are refitted using CSA tensors where the $\sigma_{22}$ axis is rotated in small steps around either the $\sigma_{11}$ or $\sigma_{33}$ axis. A clockwise rotation of $\sigma_{22}$ and $\sigma_{33}$ when viewed in the $\sigma_{11}$ vector direction (Figure 7) by 11° results in a small but statistically significant improvement of the fit ($P_F = 2\%$) (Supporting Information). When examining the same question separately for the helix and sheet residues, a $22 \pm 10°$ clockwise rotation around the $\sigma_{11}$ vector optimizes the fit between $\Delta\delta^{meas}$ and $\Delta\delta^{pred}$ values for helical residues ($P_F = 2\%$; Figure 9), but no statistically significant improvement is observed for $\beta$-sheet residues (Supporting Information). The ±10° precision was obtained by taking the difference between the angle corresponding to 22° (lowest $\chi^2$) and the angle corresponding to one standard deviation of the $\chi^2$ distribution for 4 degrees of freedom. A rotation of the CSA tensor in this direction is compatible with reports by Lee et al. for collagen[43] and Boyd and Redfield for lysozyme.[40]

**$^1$H$^N$ CSA.** For $^1$H$^N$, the commonly used approximation of an axially symmetric shielding tensor is found to be invalid, and a best fit between $\Delta\delta_i^{meas}$ and $\Delta\delta_i^{pred}$ is obtained for a tensor with $\eta \approx 1$ (Figure 6; Table 4). The least shielded $\sigma_{11}$ axis is orthogonal to the peptide plane, and consistent with previous literature data, $\sigma_{33}$ is nearly parallel to the N−H bond ($\beta_H = 8 \pm 3°$; Figure 7). The quality factor $Q$ of the correlation (Figure 7A) is 38% and the pairwise rmsd is 1.5 ppb. Assuming $\beta_H$ to be fixed, an upper limit of ±1.7 ppm random variation in the $^1$H$^N$ CSA tensor components is found, using the Monte Carlo procedure described above. Solid-state measurements indicate that the downfield change in the isotropic chemical shift of the protons for increasing hydrogen bond strength is accompanied by an increase in $^1$H$^N$ CSA.[81] This was also confirmed in solution NMR by studies of relaxation interference between $^1$H$^N$ CSA and $^1$H$^N$−$^{15}$N dipolar relaxation mechanisms.[46,47]

In contrast to $^{13}$C′ and $^{15}$N, for $^1$H$^N$ a strong correlation between $(\Delta\delta_i^{meas} - \Delta\delta_i^{pred,NMR})$ and $(\Delta\delta_i^{meas} - \Delta\delta_i^{pred,X-ray})$ is

(80) Kay, L. E.; Torchia, D. A.; Bax, A. *Biochemistry* **1989**, *28*, 8972−8979.
(81) Berglund, B.; Vaughan, R. W. *J. Chem. Phys.* **1980**, *73*, 2037−2043.

obtained ($R = 0.92$, Supporting Information). Therefore, the upper limits for the standard deviation in the principal components of the $^1H^N$ CSA tensor reported in Table 4 are believed to reflect closely the true variability.

When separately fitting residues in helical and extended conformations, the orientation and rhombicity are found to be very similar but the CSA magnitude for sheet residues is about 40% larger than for helical ones (Table 4). Considerable scatter remains in the correlation between $\Delta\delta_i^{meas}$ and $\Delta\delta_i^{pred}$ (Supporting Information), indicating that significant variation in the $^1H^N$ CSA tensor is present within the helical and $\beta$-strand subsets. No meaningful improvement in the fit was obtained when systematically rotating the $\sigma_{22}$ and $\sigma_{33}$ principal axes around $\sigma_{11}$, neither when considering all residues simultaneously, nor when considering helical and sheet residues separately (data not shown). The $^1H^N$ CSA values found in this study, $\Delta\sigma = \sigma_{11} - (\sigma_{22} + \sigma_{33})/2 = -7.2$ ppm for α-helix and $-9.9$ ppm for $\beta$-sheet, are in close agreement with the averages of the residue-specific $^1H^N$ CSA values from relaxation interference studies.[47]

## Concluding Remarks

As pointed out previously, the degree of correlation between measured and predicted $\Delta\delta_{C'}$ or $\Delta\delta_N$ can be used as a sensitive monitor for evaluating the quality of a protein structure. The remarkable agreement between measured $\Delta\delta$ values and those predicted by the NMR structure testifies to the high quality of the backbone geometry of this structure. Direct use of chemical shifts to improve a structure is more problematic, however, particularly for structures which are quite good to start with: The inherent variability of the CSA tensor is nonnegligible and refining a structure by assuming the $^{13}C'$ and $^{15}N$ CSA tensors to be uniform can introduce small systematic errors.

The large degree of variability in the $^1H^N$ CSA tensor explains the wide range in TROSY $^1H^N$ line narrowing observed in perdeuterated proteins.[48] It also is consistent with the, on average, smaller TROSY enhancements seen in helical residues compared to $\beta$-sheet. Interestingly, the smaller CSA for helical proteins compared to what was used in model calculations by Pervushin and co-workers[18] shifts the optimum field strength at which the lowest $^1H^N$ line width is obtained to even higher fields. For both helix and sheet, the large degree of rhombicity for the $^1H^N$ CSA tensor, however, results in smaller absolute enhancements than predicted for an axially symmetric tensor.

The primary uncertainties in deriving the CSA from the $\Delta\delta$ values are the deviations from the assumption of a uniform tensor, and small residual errors in the refined structure. Although the fit between the experimental $\Delta\delta$ values and the structure was much better for the NMR structure than for the X-ray structure of ubiquitin, small systematic deviations in the peptide plane orientation can occur in NMR structures refined with dipolar couplings. These minute systematic distortions can alter the best-fitted CSA components by a few percent, without increasing the scatter of the correlation. This effect was most noticible for $^{13}C'$, where the original NMR structure yielded a CSA which was nearly 4 ppm larger than for the structure obtained after fine-tuning the relative magnitudes of the various heteronuclear dipolar couplings.

As discussed in the Uncertainty in Average CSA section, variations in backbone dynamics are not a major source of scatter for the correlation plots in Figures 4−6. Nevertheless, we expected to see a small improvement in these correlations after the measured $\Delta\delta$ values were scaled by $S^{-1}$, obtained from previously reported $^{15}N$ relaxation studies.[37,82] This was not the case. Use of either set of order parameters[37,82] resulted in correlation coefficients differing by less than 0.1% from the uncorrected set. A possible explanation for this observation may be that the peptide bonds with the largest correction factors (lowest $S$) are also the ones with the largest differences between the crystal and solution structure, and the scatter for these residues is even more strongly affected by the uncertainty of their bond vector orientations. The ubiquitin solution structure itself may also be distorted in these regions because the dipolar restraints were used in the structure calculation under the assumption of uniform dynamics, i.e., without scaling.

Previously, residue-specific CSA values and tensor orientations ($\beta_N$) have been derived from $^{15}N$ relaxation studies.[23] Use of these residue-specific CSA values slightly decreased the fit of Figure 5, mainly as a result of the relatively large uncertainties reported for a subset of these CSA values.

The present study provides quantitative insight into the degree of variability of the $^1H^N$, $^{13}C'$, and $^{15}N$ CSA tensor components. For $^1H^N$, a rather large variability of ±1.7 ppm rms is found for the individual tensor components, assuming that the CSA tensor orientation remains the same. For $^{13}C'$ and $^{15}N$ only upper limits for the degree of variability are obtained, and these upper limits are also rather large (±13 ppm for $^{15}N$; ±10 ppm for $^{13}C'$). These variations are comparable to the differences between the average helix and $\beta$-sheet values of the CSA principal components reported in Tables 2 and 3. Variations in the individual tensor components are most important for cross correlation type experiments. For the common auto-correlation type $T_1$ and $T_2$ relaxation studies it is the variability in the magnitude of the CSA tensor, $\Delta\sigma$, that is most relevant. Our measurements do not provide a good measure for the degree of variation in $\Delta\sigma$ because changes of the CSA principal components from their average value are likely to be correlated to some degree. For example, for $^{15}N$ the changes in $\sigma_{22}$ and $\sigma_{33}$ tend to have opposite signs, with little net effect on $\Delta\sigma$.[33,38] In this respect, it is interesting to note that for both $^{13}C'$ and $^{15}N$ the difference in CSA magnitude between helix and sheet is rather small, whereas the change in asymmetry is substantial. Variations in the asymmetry of the CSA tensor have relatively little effect on the auto-relaxation rates, however.

In principle, it is possible to derive residue-specific values for the CSA if very accurate $\Delta\delta$ values are measured for at least two very different alignment tensors, and if the orientation of the CSA tensor is assumed to be constant. Although the orientation of ubiquitin relative to the liquid crystal director indeed can be modulated by adding a net charge to the bicelle surface,[83] we found that the change in the alignment tensor is insufficiently large to permit such individual CSA measurements at a useful degree of accuracy.

**Acknowledgment.** Work by Gabriel Cornilescu is in partial fulfillment for the Ph.D. degree at the University of Maryland, College Park, MD. We thank Stephan Grzesiek and Marco Rogowski for the sample of perdeuterated $^{13}C/^{15}N$ ubiquitin, and Frank Delaglio, Nico Tjandra, John Marquardt, Marcel Ottiger, Marius Clore, Angela Gronenborn, Rob Tycko, Attila

(82) Tjandra, N.; Feller, S. E.; Pastor, R. W.; Bax, A. *J. Am. Chem. Soc.* **1995**, *117*, 12562−12566.
(83) Ramirez, B. E.; Bax, A. *J. Am. Chem. Soc.* **1998**, *120*, 9106−9107.
(84) Wang, A. C.; Bax, A. *J. Biomol. NMR* **1993**, *3*, 715−720.
(85) Silver, M. S.; Joseph, R. I.; Hoult, D. I. *Nature* **1984**, *310*, 681−683.
(86) Grzesiek, S.; Bax, A. *J. Biomol. NMR* **1993**, *3*, 185−204.
(87) Logan, T. M.; Olejniczak, E. T.; Xu, R. X.; Fesik, S. W. *J. Biomol. NMR* **1993**, *3*, 225−231.

Szabo, Dennis Torchia, and David Weliky for many useful discussions. This work was supported by the AIDS Targeted Anti-Viral Program of the Office of the Director of the National Institutes of Health. This paper was originally intended to be included in the Molecular Physics Volume 75 issue, dedicated to Professor Richard R. Ernst on the occasion of his 65th birthday. However, at that time the discrepancy with solid state $^{13}C'$ CSA data, when using the original NMR structure (see text), could not be explained. We now dedicate it to him on the occasion of his 67th birthday.

**Supporting Information Available:** One table of ubiquitin $^{1}H^{N}-^{15}N$ dipolar couplings; one table with $^{1}H^{N}$, $^{15}N$, and $^{13}C'$ shifts at 17 °C; one table with $^{1}H^{N}$, $^{15}N$, and $^{13}C'$ chemical shift differences between aligned and isotropic states (corrected for the temperature dependence); one table with the $^{1}H^{N}$, $^{15}N$, and $^{13}C'$ temperature factors in human ubiquitin; one figure correlating best-fitted with experimental $^{1}H^{N}-^{15}N$ dipolar coupling values for the NMR structure (Figure 1A) and the X-ray structure (Figure 1B) of ubiquitin; one figure correlating best-fitted with experimental $\Delta\delta_{C'}$ values for all helical (Figure 2A) and for all $\beta$-sheet residues (Figure 2B) in the ubiquitin X-ray structure; one figure correlating best-fitted with experimental $\Delta\delta_{N}$ values for helical (Figure 3A) and for $\beta$-sheet residues (Figure 3B); one figure correlating best-fitted with experimentally obtained $\Delta\delta_{H}$ values for helix (Figure 4A) and $\beta$-sheet (Figure 4B); one figure correlating $\Delta\delta_{i}^{pred} - \Delta\delta_{i}^{meas}$ values for the 1.8-Å X-ray structure with those obtained with the NMR structure for $^{13}C'$ (Figure 5A), $^{15}N$ (Figure 5B), and $^{1}H$ (Figure 5C); one figure showing the $\chi^2$ of the fit between $\Delta\delta(^{15}N)$ as a function of the rotation angle of the CSA tensor about $\sigma_{11}$ for all residues (Figure 6A) and only $\beta$-sheet residues (Figure 6B) (PDF). This material is available free of charge via the Internet at http://pubs.acs.org.

JA0016194